An IR image processing approach for characterising combustion instability

M. CHIMENTI[1], C. DI NATALI[2], G. MARIOTTI[2], E. PAGANINI[2], G. PIERI[1], O. SALVETTI[1]

[1] Istituto di Scienza e Tecnologie dell'Informazione del CNR

Via G. Moruzzi 1, 56124 – Pisa

[2] ENEL Produzione Ricerca

Via Andrea Pisano 120, 56122 – Pisa

Corresponding author: Ovidio Salvetti, ISTI – CNR, Via G. Moruzzi 1, 56124 – Pisa – ITALY

ABSTRACT

The paper presents a first approach to the analysis of the dynamic behaviour of a premixed hydrogen/air jet flame using near-IR imaging. In this kind of flames spectral lines are observed in the infrared, visible, and ultraviolet regions; emissions of visible light are however not so strong as in other wavelengths, especially in the near-infrared and infrared portions of the spectrum. Using a video camera, coupled with an optical filter, it is possible to capture images of the flame in a burner and then acquire sequences of images of the near-infrared emission during the combustion process. In this work, carried out in the frame of a collaboration between ENEL Produzione – Ricerca and ISTI – CNR, we propose a method suitable to process and analyse maps of near-infrared emissions in order to characterize the flame morphology and compute geometric and densitometric features useful to describe the combustion dynamics. The map of the emissions presents in some cases different unconnected sources with interesting distribution. In our analysis, we considered two different layers: the single images, as a distribution of near-IR emission, and the complete sequence of images in a dynamical evolution of the whole process.

KEYWORDS: Hydrogen flame, Infrared Imaging, Image Processing

Introduction

The increasing attention of the regulatory bodies towards the environmental impact of the combustion processes, as well as the significant penetration of the natural gas into the fuel market, led to the diffusion of combustion systems capable to limit the pollutant emission by means of the lean premixed combustion technique. The drawback of this approach is the tendency of this kind of flames towards the instability, which can be mainly of two types: acoustic oscillation, or blow-out of the flame. These instabilities differentiate in frequencies; acoustic oscillations occur at frequencies of 100Hz or higher, while blow-out occurs at frequencies around 10Hz. Very often also a different flame morphology is associated to the phenomena. Hence the interest for the study of the flame dynamics and morphology has been increased, and this is at present one of the most explored areas of research for the combustion community [1].

It is already long time since this optical techniques provided by chemiluminescence optical sensors (phototubes and cameras) are used in the studies of combustion diagnosis, due to their real time and non-invasive measurements, to the continuous technological development, to the close correlation between the combustion process and the light absorption-emission phenomenon; and also because there is a reasonable expectation that they could be implemented in the near future in on industrial plants [2], [3].

Using this technique, we can observe the spontaneous emission of electromagnetic radiation by some radicals or molecules generated during the combustion process decaying from the excited status to the basic one. Since the decaying time is much shorter than the characteristic time of the diffusive or convective motions present in the flame, it is possible to use this technique to study the flame dynamic. In particular the OH* and CH* emission can be interpreted as an indicator of the heat volumetric release and of the spatial distribution of the flame surface.

In a previous research carried out by the authors [4], the problem of acoustic oscillation instability diagnosis was faced by studying the CH* radical emission observable at 425 nm wavelength. In that

case, the need to deal with low intensity emissions and fast dynamics, forced to the development of a dedicated high speed and high resolution camera for the acquisition of the optical signals [4].

More recently similar studies have been extended to hydrogen flames, not only because they usually have a much simpler chemical structure than flames of fossil fuels, hence allowing to operate in simpler conditions, but also because an increasing availability of this fuel on the market is expected, due to its characteristics of cleanness.

Differently form the methane flame, which presents relevant peaks even in the visible range, the spectrum of hydrogen flames is characterised by a strong emission in the UV range (in particular the 310 nm line is still present, linked to the emission of the OH* radicals) and in the near-infrared and infrared portions of the spectrum, due to the emission of the water molecules. In the visible range, the only regions with relevant light emission are the 590 nm line (due in part to the oxygen molecules, but mainly to the spurious presence of sodium atoms in the gas stream or on the metal surfaces) and the region above 700 nm, leading to the typical orange-red aspect of the flame. It appears therefore interesting to approach the study of the flame dynamics and morphology coupling the analysis of the UV and of the near-IR regions.

In our study, we considered two different layers of analysis: the single images, as a distribution of the near-IR emission, and the complete sequence of images, as the dynamical evolution of the whole combustion process.

Using a CCIR near-IR sensitive camera, coupled with a proper optical filter to cut the visible light spectrum, dynamic sequences of images were acquired of a laboratory hydrogen flame to study its morphology, with the aim of individuating characteristic parameters able to characterize and identify each combustion state and then exploitable to differentiate between a stable combustion from an instable one, in this case defined by a blow-out.

Preliminary results showed that the developed technique is effective and that it should be taken into consideration for the implementation of real-time monitoring of the combustion processes.

Material and Methods

An image acquisition campaign has been carried out at the Enel laboratory in Livorno, where a premixed hydrogen/air jet flame combustor is available.

The image sequences were obtained using a CCIR near-IR sensitive camera at 50 fps rate. Each image had 768x536x8 bits/pixel spatial resolution. A zoom was mounted on the camera in order to obtain different magnitudes of the shot scene.

The image processing procedure consisted of a first phase for noise reduction (image pre-processing) and a second one for the extraction of basic morphological parameters from selected regions of interest useful to describe the flame dynamics (in particular, flame area and perimeter).

Image processing procedure

Once a sequence has been acquired, in order to enhance the quality of the images, a frame-by-frame digital filtering is performed to reduce the electronic noise introduced by the digitisation equipment. In this stage of the procedure, also a *cropping* operation on the whole sequence is applied to eliminate the useless information in the images. This operation is performed taking into account some known characteristics of the scene, as in particular the symmetric-like property of the flame with respect to the burner centre. In this way, a large part of the background in each image can be cut without affecting data integrity, so obtaining a new highly compressed data set.

After cropping, digital filtering is applied to the dataset in order to reduce instrumental noise: this operation is performed implementing a Wiener filter [5]. The Wiener filter is the MSE-optimal stationary linear filter for images degraded by additive noise and blurring. Calculation of the Wiener filter requires the assumption that the signal and noise processes are second-order stationary (in the random process sense). Wiener filter is usually applied in the frequency domain. Given a degraded flame image $x(n,m) \in S$, S = acquired image sequence, the Discrete Fourier Transform (DFT) is computed to obtain $X(u,v)$. The original image spectrum is estimated by taking the product of $X(u,v)$ with the Wiener filter $W(u,v)$: $\hat{O}(u,v) = W(u,v)X(u,v)$.

Considering that in our case no blurring component is relevant, the filter W is computed as follows:

$$W(u,v) = \frac{P_I(u,v)}{P_I(u,v) + \sigma_n^2}$$

where,

$P_I(u,v)$ = power spectrum of the image obtained by taking the Fourier transform of the image autocorrelation

σ_n^2 = noise variance.

Finally, the filtered image is obtained by performing the DFT^{-1}.

In this case, when the image variance is high the filter smoothes slightly, while when it is low the filter implements a heavier smoothing. This adaptive filtering results more selective with respect to other linear filters and at the same time it preserves the edges in the images and other high frequency elements. In order to completely eliminate the *granular* noise characterising the flame images, we chose to perform successive filtering (3 times, experimentally defined).

Image segmentation

After filtering, an image segmentation is necessary to isolate only the interesting regions. This operation allows to obtain new images where only few pixels remain with their grey level unchanged on a uniform *black* background. Segmentation is performed by applying a threshold operator on the grey level histograms of the images.

In order to characterise the flame morphology more regions can be considered, i.e. more threshold values, in every image (see Figure 1), like the region corresponding to the full emission part of the flame or that relative to the flame front.

The threshold value T_i is computed as a function of few statistical parameters extracted from the intensities distribution, i.e. the mean value, μ, and the standard deviation, σ, as follows:

$$T_i = \mu + (K \times \sigma), \text{ where } K \in \left[-\frac{\mu}{\sigma}, \frac{255 - \mu}{\sigma} \right].$$

To give a first morphological characterisation of a segmented region, we chose simple geometric parameters, like area and perimeter, easily computable and then suitable to be implemented also in real-time. Moreover, the new values of mean and standard deviation of the regions themselves were also computed.

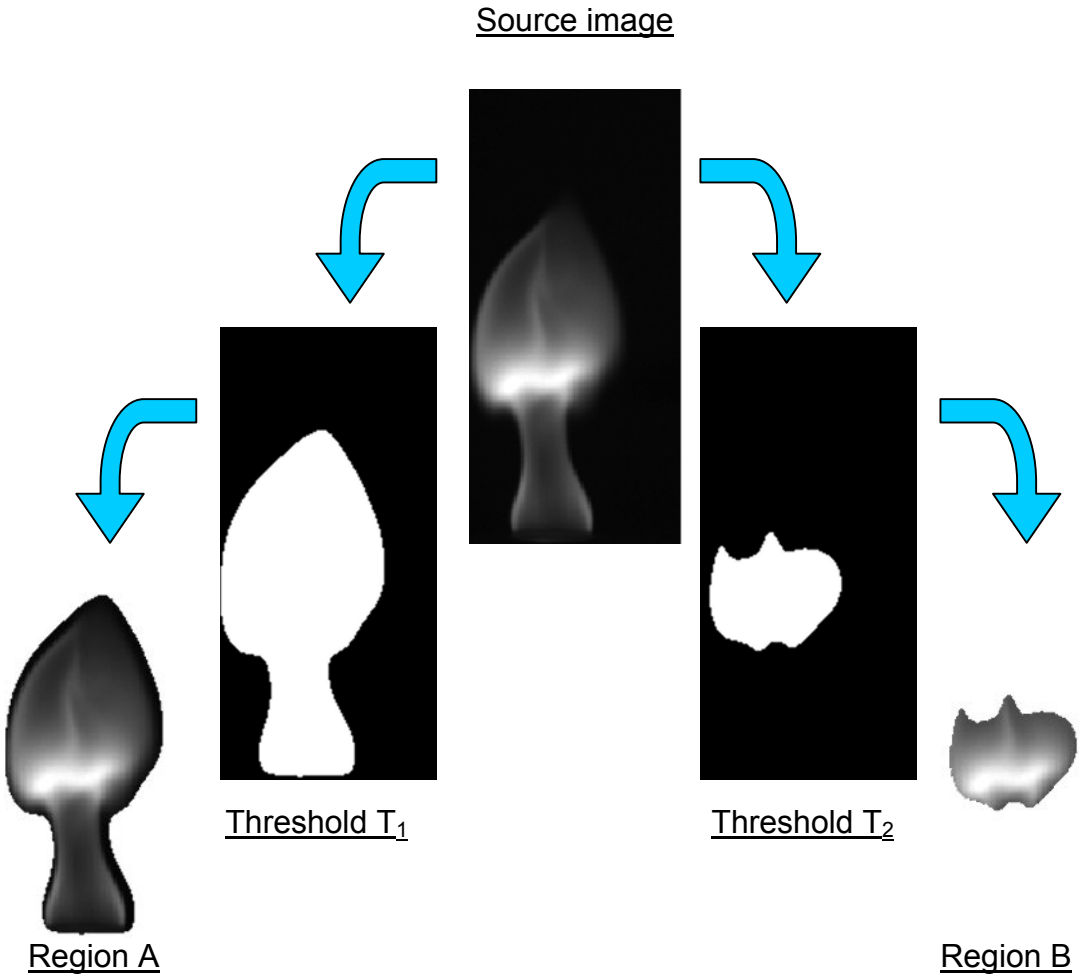

Figure 1: Source image and its segmentations in two regions.

Figure 2 shows the selection of the threshold regarding the extraction of region A.

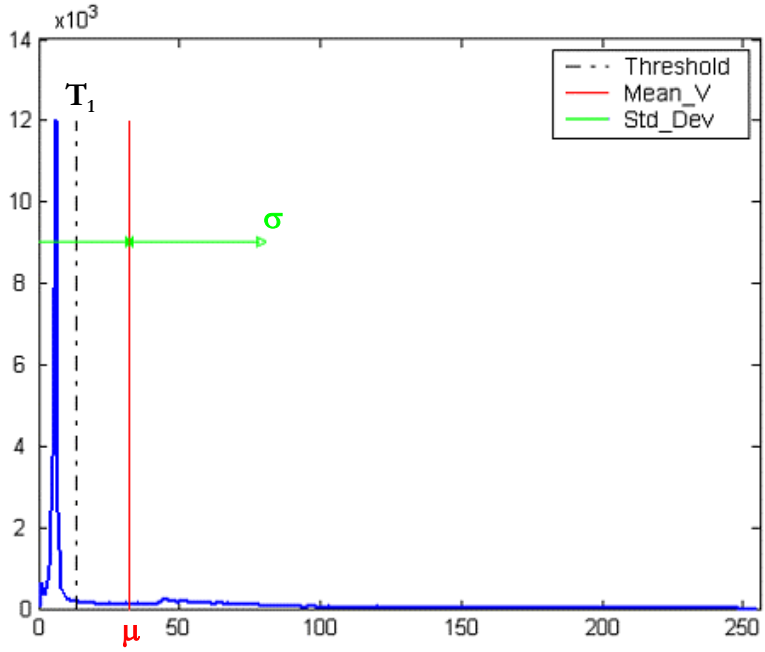

Figure 2: The threshold T_1 is computed as a function of the mean and standard deviation of the source image histogram with K= -0.4.

Morphological Characteristics Extraction

The first operation performed on the segmented image is the extraction of the edge belonging to the region. To this end, an isotropic gradient operator [6] is applied in order to obtain a binary *edge map*, *f*, as shown in Figure 3a for region A.

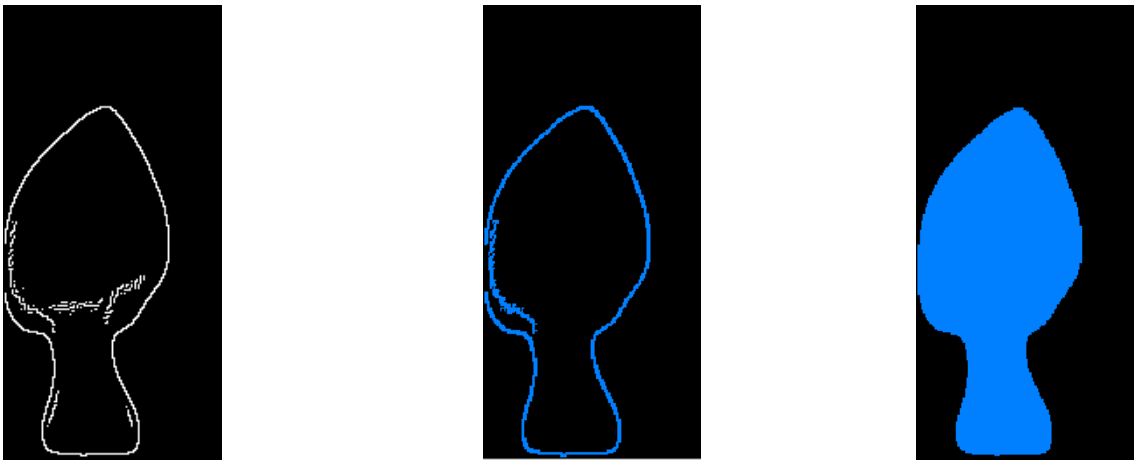

(a) (b) (c)

Figure 3: Binary edge map relative to Region A (a). Edge map after the flame boundary detection (b). Connected region relative to region A (c).

Finally, a dilation morphological operator ($\oplus$) is applied on f [7] to obtain a continuous and closed edge line that defines the boundary of the region. The operation is performed computing a new image (see Figure 3b) $h = f \oplus s$,

where,

$$s = \begin{bmatrix} 1 & 1 \\ 1 & 0 \end{bmatrix}$$

$$h_{i,j} = \begin{cases} 1 & \text{if } f_{i+\mu,j+\nu} = 1 \text{ for at least one } (\mu,\nu) \in s \\ 0 & \text{otherwise} \end{cases}$$

i,j = co-ordinates of a generic pixel in the image.

At this point, the perimeter *P* and the area *R* of the region (Figure 3c) can be computed as follows:

$$P = \sum_{i,j} h_{i,j}$$

$$R = \sum_{i,j} t_{i,j}, \text{ where } t_{i,j} = 1 \quad \text{if} \quad i,j \in \text{Region}$$

Results

A series of eight different acquisitions was performed:

- two with a pure diffusive hydrogen flame, with near-IR filter;
- two acquisitions in the same conditions but without the coupled near-IR filter;
- two acquisitions with a partially premixed air-hydrogen mixture with a lower amount of air (with near-IR filter);
- two acquisitions again in partially premixed conditions, with a higher amount of air (with near-IR filter) (see Table 1).

The duration of each acquisition is 6 s.

Acquisitions	Flame conditions	Filter
1-2	Pure diffusive flame (H_2 13 ml/min)	R69 Filter (>735nm)
3-4	Pure diffusive flame	No filter

5-6	Partially pre-mixed H_2-Air (rich mixture)	R69 Filter (>735nm)
7-8	Partially pre-mixed H_2-Air (lean mixture)	R69 Filter (>735nm)

Table 1: Measurements performed.

The near-IR filter characteristics are shown in Figure 4, which compares the filtered flame spectrum and the not-filtered one. The figure shows that the filtered spectrum well preserves the emission from the water molecules in the range from 700 to 900 nm, while the 590 nm peak is dropped. This peak is presumably due to the presence of sodium traces in the mixture; this element does not participate to the combustion process, but its strong randomly varying emission induces a significant noise in the signals.

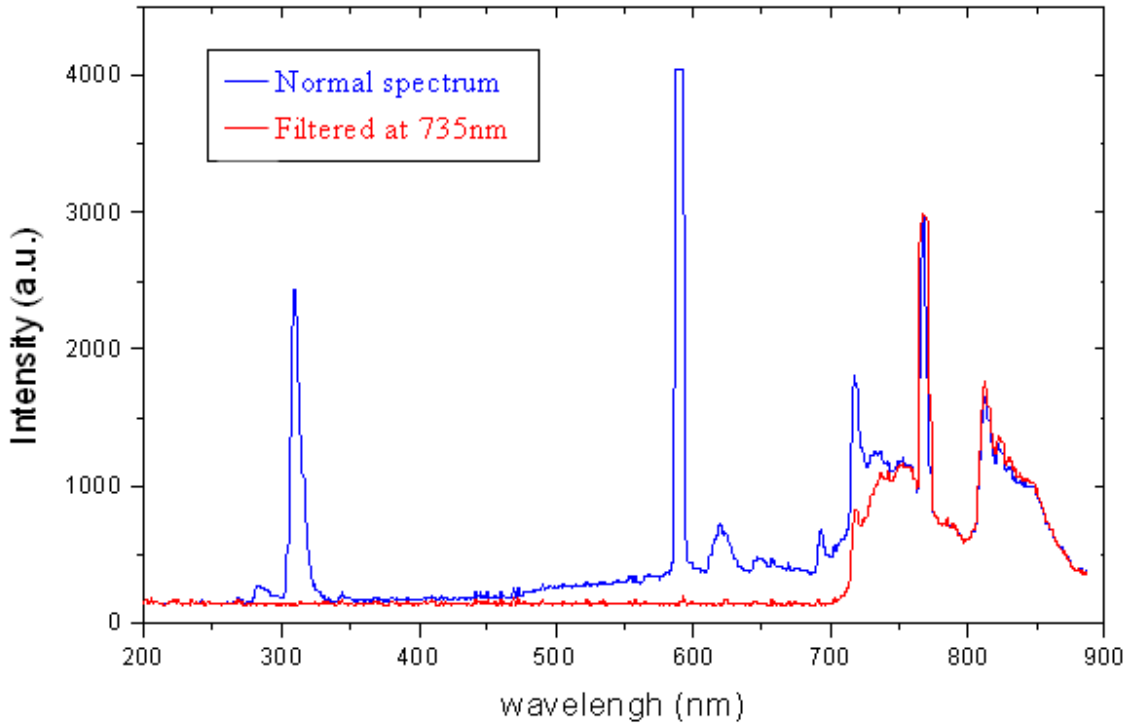

Figure 4: Spectral response of the IR filter compared with the behaviour of a not-filtered response taken at a close different time, for a hydrogen flame.

The effect of cutting the 590 nm peak is well shown in Figure 5, Figure 6 and Figure 7. Figure 5 shows the spatial standard deviation calculated in each image for the whole recorded period (in the *x* axis is reported the recording time). Both curves (with and without filter) put in clear evidence the oscillation related to the dynamic of the flame, but, in the case with the filter, the mean value of the standard

deviation goes down in a significant way. This is due to the suppression of the random component of the Na emission. The same effect is shown in Figure 6 for the comparison of the perimeter measures between a filtered sequence and a not filtered one.

Similarly, Figure 7 shows for each pixel of the image the highest detected standard deviation; this picture can be therefore considered the envelope of the flame shape. When using the filter the dispersion is much lower and the shape of the flame is well evidenced.

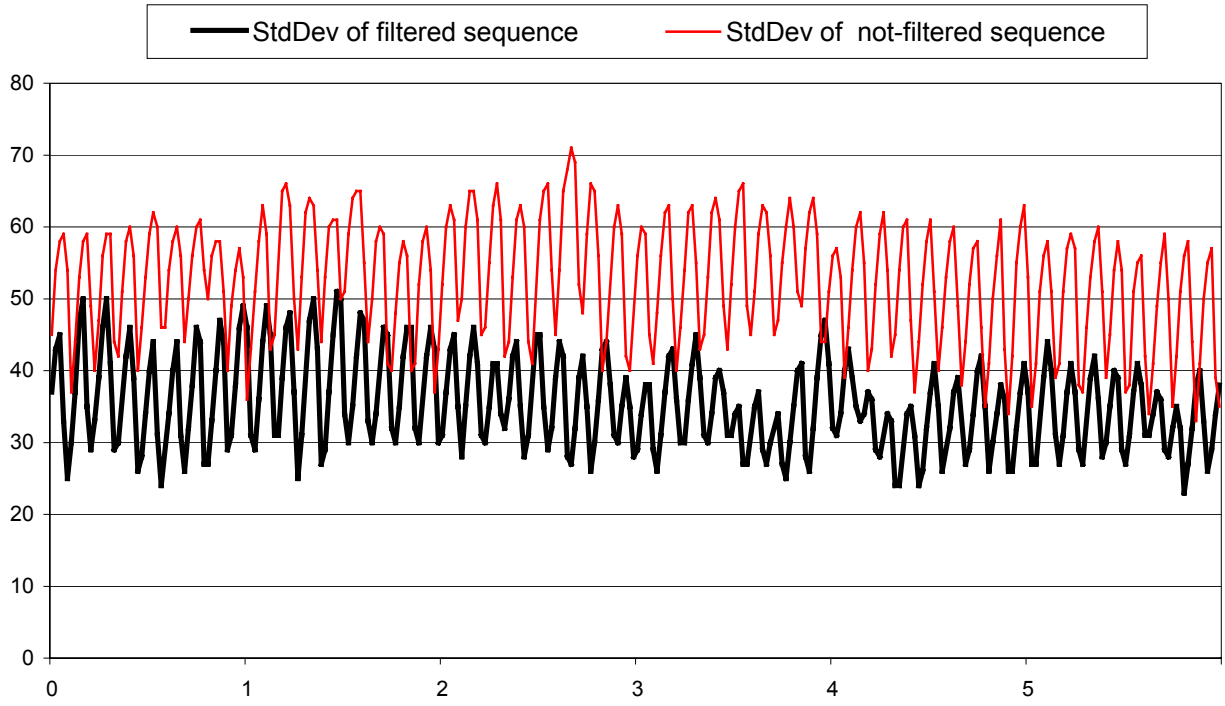

Figure 5: Filtered sequence Standard Deviation vs the not filtered one.

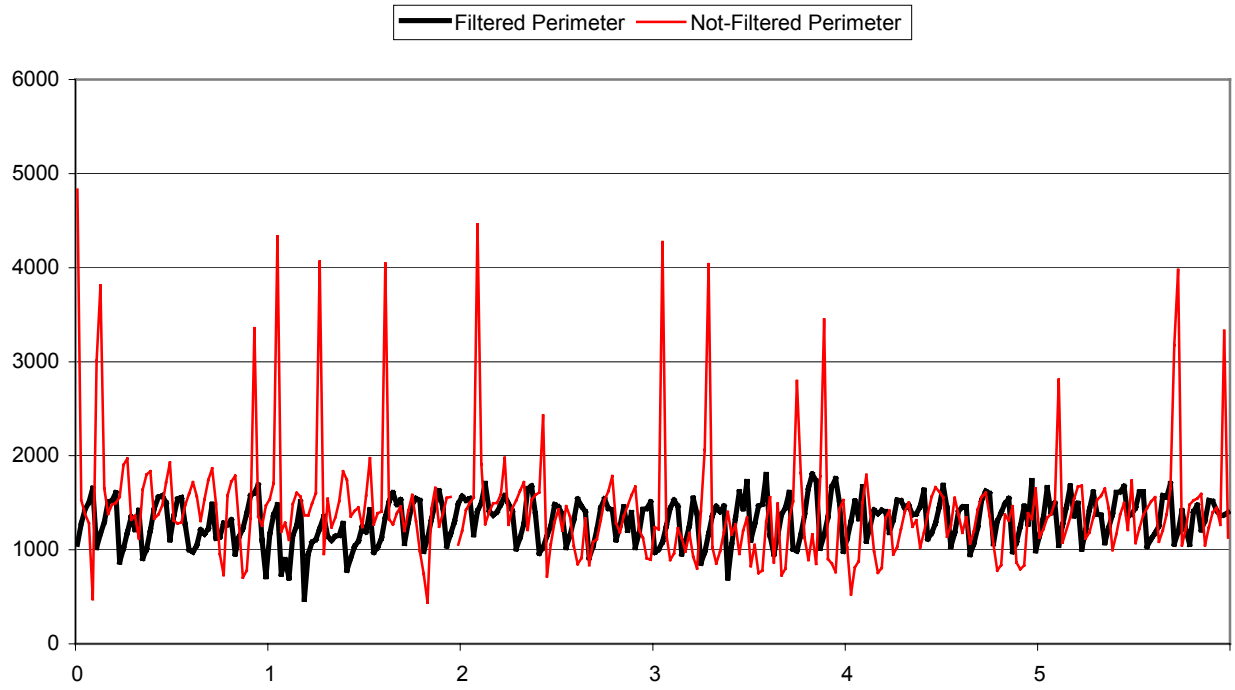

Figure 6: Perimeter of the filtered sequence vs the perimeter of the not filtered one.

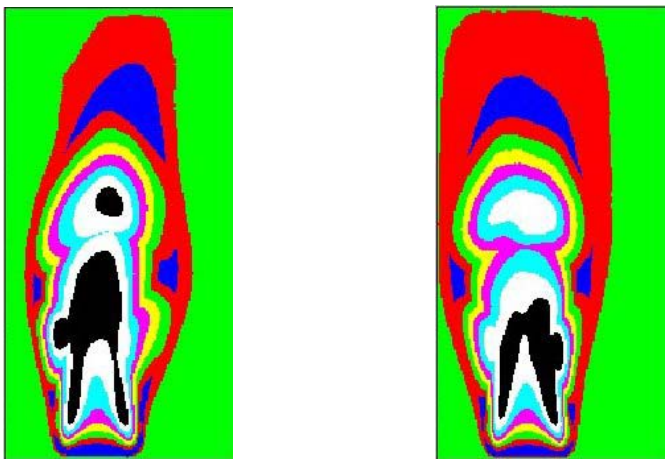

Figure 7: Pseudo-colour map comparison of a filtered (left) and not filtered (right) flame.

Finally in Figure 8 a comparison between three different combustion conditions, through the area measure is performed. The figure shows that it is possible to associate different values of the area to different flame conditions; this aspect will have to be deeply investigated in the future to verify the possibility to use this technique as a diagnostic method in a real combustor.

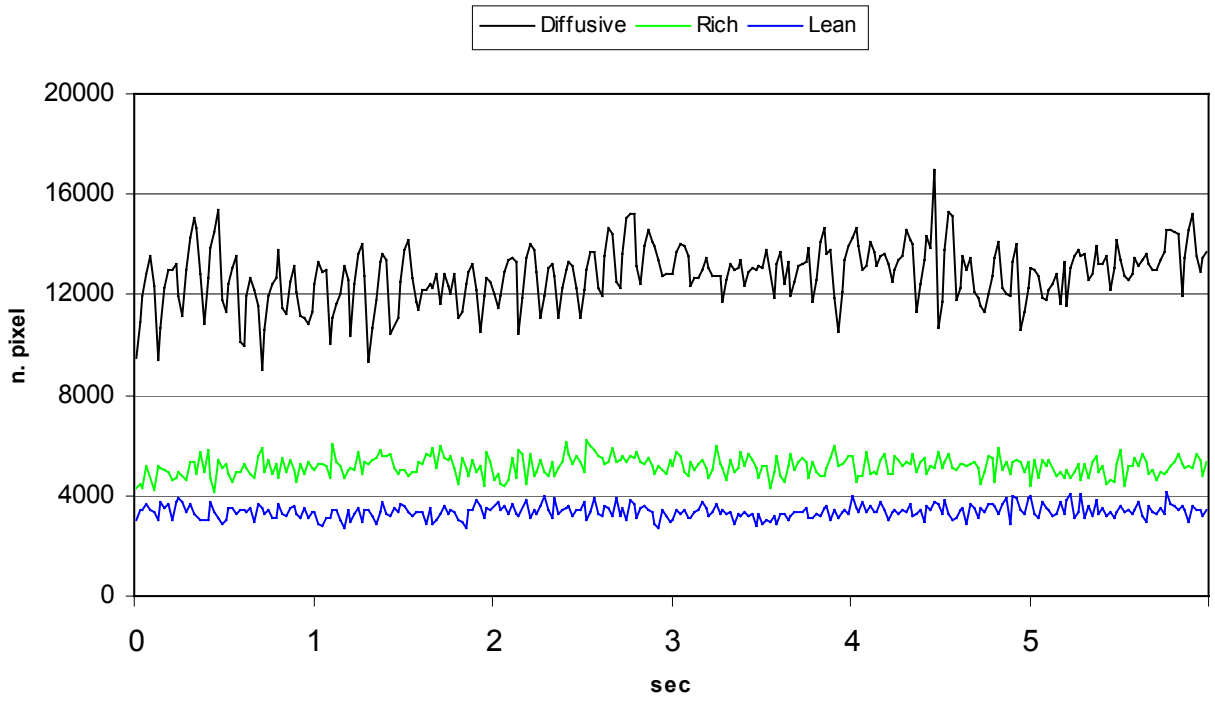

Figure 8: Dynamical analysis of the Area parameter of image sequences, for 3 different combustion conditions.

Conclusions

The comparison between filtered and unfiltered images shows that the unfiltered ones are characterized by the presence of a higher standard deviation, due to the presence of noise in the visible region and in particular due to sodium emission. The filtered images, which mainly represent the spatial distribution of the high temperature reaction product (water), provide relevant information about the global shape of the flame, and allow to individuate the region of the quenching due to the entrainment of the surrounding low temperature gas. On the contrary, signals (and eventually images) in UV range are to be preferred for the characterization of the flame front dynamics, since they are linked to emission of the OH* radicals preferentially present in the region of high reaction rate.

As far as the dynamic aspects are concerned, the characteristics of the employed camera do not allow to capture information about phenomena occurring at acoustic frequencies; it is however able to detect low frequency oscillations, typical of pre-blow out instabilities. Also from this point of view, the work opens interesting perspectives, which we can rely on.

Acknowledgments

The authors would greatly thank Aurelio Cipriano, Enel, for his valuable contribution in the operation of the experimental burner and of the related instrumentation.

References

[1] S. Candel "Combustion Dynamics and Control: Progress and Challenges", 2002. 29th Symposium on Combustion.

[2] Y. Ikeda, J. Kojima, S. Amano, T. Nakajima "Time Series Equivalence Ratio Measurement in Turbulent Flames", 2002. 40th Aerospace Sciences Meeting & Exhibit.

[3] N. Docquier, F. Lacas, S. Candel "Closed loop equivalence ratio control of premixed combustors using spectrally resolved chemiluminescence measurements", 2002. 29th Symposium on Combustion.

[4] C. Di Natali, "Messa a punto di tecniche di misura e di analisi per la caratterizzazione delle instabilità di combustione", 2002. Technical report, ENEL Produzione – Ricerca, n° ENELP/RIC/RT-2002/…/0-IT+RT.RIC.PI

[5] Rafael C. Gonzalez, and Paul Wintz, Digital Image Processing, 2nd Edition, Addison Wesley, 1987.

[6] I. Sobel, "An Isotropic 3 3 images gradient operator", 1990. In H. Freeman, Ed., Machine Vision of Three-Dimensional Scenes, pp. 376-379, Academic Press.

[7] J. Serra, "Image Analysis and Mathematical Morphology", 1982. (Academic, London).

Figure captions

Figure 1: Source image and its segmentations in two regions.

Figure 2: The threshold T_1 is computed as a function of the mean and standard deviation of the source image histogram with K= -0.4.

Figure 3: Binary edge map relative to Region A (a). Edge map after the flame boundary detection (b). Connected region relative to region A (c).

Figure 4: Spectral response of the IR filter compared with the behaviour of a not-filtered response taken at a close different time, for a hydrogen flame.

Figure 5: Filtered sequence Standard Deviation vs the not filtered one.

Figure 6: Perimeter of the filtered sequence vs the perimeter of the not filtered one.

Figure 7: Pseudo-colour map comparison of a filtered (left) and not filtered (right) flame.

Figure 8: Dynamical analysis of the Area parameter of image sequences, for 3 different combustion conditions.

Tables

Table 1: Measurements performed